Cite as: S. Ota *et al.*, *Science* 10.1126/science.aav3136 (2019).

Response to Comment on "Ghost cytometry"

Sadao Ota[1,2]*, Ryoichi Horisaki[3,4], Yoko Kawamura[1], Masashi Ugawa[1,2,5], Issei Sato[1,2,5], Hiroaki Adachi[1], Satoko Yamaguchi[2], Katsuhito Fujiu[2], Kayo Waki[2], Hiroyuki Noji[2]

[1]ThinkCyte Inc., 7-3-1 Hongo, Bunkyo-ku, Tokyo 113-8654, Japan. [2]University of Tokyo, 7-3-1 Hongo, Bunkyo-ku, Tokyo 113-8654, Japan. [3]Department of Information and Physical Sciences, Graduate School of Information Science and Technology, Osaka University, 1-5 Yamadaoka, Suita, Osaka 565-0871, Japan. [4]JST, PRESTO, 4-1-8 Honcho, Kawaguchi-shi, Saitama 332-0012, Japan. [5]RIKEN AIP, Nihonbashi 1-chome Mitsui Building, 15th floor, 1-4-1 Nihonbashi, Chuo-ku, Tokyo 103-0027, Japan.

*Corresponding author. Email: sadaota@solab.rcast.u-tokyo.ac.jp

Di Carlo *et al.* comment that our original results were insufficient to prove that the ghost cytometry technique is performing a morphologic analysis of cells in flow. We emphasize that the technique is primarily intended to acquire and classify morphological information of cells in a computationally efficient manner without reconstructing images. We provide additional supporting information, including images reconstructed from the compressive waveforms and a discussion of current and future throughput potentials.

Ghost cytometry (GC) performs a direct analysis of compressive imaging waveforms and thereby substantially relieves the computational bottleneck hindering the realization of high-throughput cytometry based on morphological information (*1*). The comments by Di Carlo *et al.* argue against a number of our conclusions (*2*), but given the restricted length allowed for this response, we will address what we consider the most important points.

As a response to the request in (*2*) for more information regarding the image reconstruction capability of GC, we provide results of image acquisition and its analysis in a high-speed "imaging" mode. As shown in Fig. 1A, we performed motion-driven compressive sensing of 600 fluorescent beads, consisting of 300 each of two different sizes and intensities, which were hydrodynamically focused in flow. The acquired waveforms were processed to build a library of reconstructed images, from which singlet bead images were analyzed to determine bead diameter and total fluorescence intensity. Histograms (Fig. 1B) of both the diameter and fluorescence intensity produce a characteristic bimodal distribution with peaks at the expected diameters and intensities, confirming the capability of GC to perform image reconstruction–based analysis. Comparison of these histograms with those of forward scatter and total fluorescence intensity measurements of the same bead samples using a standard flow cytometer (Fig. 1C), gated to include only singlets, shows consistency.

As to the sensitivity of the ghost imaging in flow, we performed peak signal-to-noise ratio (PSNR) measurements of fluorescent beads in the same polydimethylsiloxane (PDMS) device used in the paper (*1*). For two example reconstructed bead images, using a reference bead image taken by a conventional microscope, we obtained moderately good PSNRs of 28.8 dB and 29.0 dB (Fig. 1D). It is also noteworthy that, in general, image reconstruction in compressive sensing is computationally costly, and image qualities are affected by calibration errors rather than the theoretical limit. GC bypasses both of these issues by using machine learning directly on the acquired waveform. To further clarify the remark on the performance metrics (*2*), we mentioned the PSNR of the non-flow demonstration within the introduction of a new imaging method in the paper (*1*), not as the overall performance of the integrated flow systems.

Regarding the separable clustering of MCF-7 and MIA PaCa-2 cells in the scatterplot of waveform length and peak intensity, we acknowledge that feature extraction from our GC waveforms can be helpful in classification of cells, especially if there is a priori knowledge of their critical characteristics. The same can be said of feature extraction from two-dimensional (2D) images. However, in both cases limiting the analysis to only one or two data features results in only partial usage of the available information. Analysis using the entirety of the morphological information encoded in the compressive signal improves classification performance relative to analysis based solely on waveform width and peak intensity. In the case of MCF-7 and MIA PaCa-2 cells, using the same dataset used in figure 4D of (*1*), the area under the curve (AUC) obtained for the waveform-based analysis showed superior performance of 0.971, whereas that for the two-feature–based analysis was 0.935 [receiver operating characteristic (ROC) curve of each is shown in Fig. 2A]. Furthermore, to control for differences in waveform length or height due to cell size or velocity, we

Downloaded from http://science.sciencemag.org/ on November 19, 2019

repeated the support vector machine (SVM) analysis using a restricted data set consisting of only the cells with similar values of both waveform width and height (Fig. 2B, red rectangle). Critically, the AUC for the waveform-based analysis of cells with similar waveform width and height was 0.930, whereas that for the two-feature–based analysis was only 0.626 (Fig. 2C). This result supports the conclusion that GC performs classification based on the detailed morphological features encoded in the waveform.

Regarding throughput, as described in the paper (*1*), we evidently calculated the throughput as a speed of flow-driven transfer of image information from cells to an analysis system, that is, the inverse of the width of the signal waveform from a single cell: throughput = 1/[width of signal (s per cell)] = flow speed (m/s)/[cell size + illumination length (m per cell)]; 1/100 μs per cell ≈ 10,000 cells/s and 1/300 μs per cell ≈ 3000 cells/s. This assumes an ideal condition wherein the cell-cell interval is maintained constant (*3*, *4*) and is equal to the cell size plus the length of the illumination field. This definition, or its equivalent in different contexts, is commonly accepted in cytometry and imaging cytometry (*5*–*8*) and represents the maximum possible throughput of the system under an assumption of observing a single cell at a time. In our work (*1*), we introduced a novel imaging technique driven by the motion of objects and, therein, its acquisition speed, which is governed by the flowing speed of objects, limits the throughput of the entire system. Therefore, we reasonably adopted the throughput definition based on the flow-governed acquisition speed of image information throughout all the analysis.

Nonetheless, we acknowledge that the random spacing of cells entering the analytical region limits the "throughput" suggested by Di Carlo *et al.* as the input cell rate minus the abort rate ["throughput" does not necessarily exclude the abort rate (*9*, *10*)]. In the sorting experiment in figure 5 of (*1*), the input cell rate was adjusted one order of magnitude lower than the throughput defined by the acquisition speed to prevent the overlap of waveforms. Integrating powerful fluidic cell-ordering techniques holds great potential to directly overcome this issue (*3*, *4*). Meanwhile, the structured illumination in the current embodiment is designed specifically to be long enough to facilitate image reconstruction for the purpose of demonstrating the principles of the technique. In future embodiments of GC optimized for morphologic analysis without the need for image reconstruction, the waveform length can be substantially reduced and the coincidence abort rate can be subsequently decreased. In addition, in the case where more than a single object enters the illumination at once, the multiple objects in an image can be recovered as shown in figure 2 of (*1*) and thus possibly can be analyzed individually. This indicates that overlapped waveforms do not necessarily limit throughput, potentially even without image reconstruction. We lastly answer the question "Why were so few cells analyzed?" We analyzed only a part of the sorted cell solutions to reduce the time required for measurements and adjusted the total amount of cell data in the histograms so that the number of positive cells before and after sorting appears equivalent.

Even in standard 2D or 3D microscopy, machine learning classifiers may be relying on simple features such as particle size or intensity, or recognizing features that are inconspicuous to the human eye. Our approach takes advantage of the ability of machine learning to recognize indistinct features for classifying cells upon an imaging modality incomprehensible to humans. We believe that the importance of using modalities that classify cells on the basis of the most differentiating, rather than the most human-suitable, information will be acknowledged not only in imaging flow cytometry but in wider areas of science (*11*, *12*) and will rapidly disseminate. Further evidence supporting the image-free approach for morphologic analysis and answers to other questions raised by Di Carlo *et al.* (*2*) can be found in other reports (*13*, *14*).

REFERENCES

1. S. Ota, R. Horisaki, Y. Kawamura, M. Ugawa, I. Sato, K. Hashimoto, R. Kamesawa, K. Setoyama, S. Yamaguchi, K. Fujiu, K. Waki, H. Noji, Ghost cytometry. *Science* **360**, 1246–1251 (2018). doi:10.1126/science.aan0096 Medline
2. D. Di Carlo, F. Arai, K. Goda, T. J. Huang, Y.-H. Lo, N. Nitta, Y. Ozeki, K. Tsia, S. Uemura, K. K. Y. Wong, Comment on "Ghost cytometry". *Science* **364**, eaav1429 (2018). doi:10.1126/science.eaav1429
3. W. Lee, H. Amini, H. A. Stone, D. Di Carlo, Dynamic self-assembly and control of microfluidic particle crystals. *Proc. Natl. Acad. Sci. U.S.A.* **107**, 22413–22418 (2010). doi:10.1073/pnas.1010297107 Medline
4. D. Di Carlo, D. Irimia, R. G. Tompkins, M. Toner, Continuous inertial focusing, ordering, and separation of particles in microchannels. *Proc. Natl. Acad. Sci. U.S.A.* **104**, 18892–18897 (2007). doi:10.1073/pnas.0704958104 Medline
5. E. D. Diebold, B. W. Buckley, D. R. Gossett, B. Jalali, Digitally synthesized beat frequency multiplexing for sub-millisecond fluorescence microscopy. *Nat. Photonics* **7**, 806–810 (2013). doi:10.1038/nphoton.2013.245
6. Y. Han, Y.-H. Lo, Imaging cells in flow cytometer using spatial-temporal transformation. *Sci. Rep.* **5**, 13267 (2015). doi:10.1038/srep13267 Medline
7. Y. Han, Y. Gu, A. C. Zhang, Y.-H. Lo, Review: Imaging technologies for flow cytometry. *Lab Chip* **16**, 4639–4647 (2016). doi:10.1039/C6LC01063F Medline
8. F. M. Rocca, J. Nedbal, D. Tyndall, N. Krstajić, D. D. Li, S. M. Ameer-Beg, R. K. Henderson, Real-time fluorescence lifetime actuation for cell sorting using a CMOS SPAD silicon photomultiplier. *Opt. Lett.* **41**, 673–676 (2016). doi:10.1364/OL.41.000673 Medline
9. D. Fox, "XDP Electronics Whitepaper Analysis of Electronic Yield," Beckman Coulter, A-11583A (2007).
10. S. H. Cho, C. H. Chen, F. S. Tsai, J. M. Godin, Y.-H. Lo, Human mammalian cell sorting using a highly integrated micro-fabricated fluorescence-activated cell sorter (microFACS). *Lab Chip* **10**, 1567–1573 (2010). doi:10.1039/c000136h Medline
11. E. M. Christiansen, S. J. Yang, D. M. Ando, A. Javaherian, G. Skibinski, S. Lipnick, E. Mount, A. O'Neil, K. Shah, A. K. Lee, P. Goyal, W. Fedus, R. Poplin, A. Esteva, M.

Downloaded from http://science.sciencemag.org/ on November 19, 2019

Berndl, L. L. Rubin, P. Nelson, S. Finkbeiner, In silico labeling: Predicting fluorescent labels in unlabeled images. *Cell* **173**, 792–803.e19 (2018). doi:10.1016/j.cell.2018.03.040 Medline

12. C. Ounkomol, S. Seshamani, M. M. Maleckar, F. Collman, G. R. Johnson, Label-free prediction of three-dimensional fluorescence images from transmitted-light microscopy. *Nat. Methods* **15**, 917–920 (2018). doi:10.1038/s41592-018-0111-2 Medline
13. S. Ota, R. Horisaki, Y. Kawamura, I. Sato, H. Noji, Imaging cytometry without image reconstruction (ghost cytometry). arXiv 1903.12053 [eess.IV] (27 March 2019).
14. H. Adachi, Y. Kawamura, K. Nakagawa, R. Horisaki, I. Sato, S. Yamaguchi, K. Fujiu, K. Waki, H. Noji, S. Ota, Use of ghost cytometry to differentiate cells with similar gross morphologic characteristics. arXiv 1903.09538 [q-bio.QM] (22 March 2019).
15. S. Ota *et al*., Dataset for "Response to Comment on 'Ghost cytometry'." Zenodo (2019). doi:10.5281/zenodo.2602483

ACKNOWLEDGMENTS

Funding: Supported by JST-PRESTO, Japan, grants JPMJPR14F5 (S.O.), JPMJPR17PB (R.H.), and JPMJPR1302 (I.S.) and partially supported by funds of a visionary research program from Takeda Science Foundation, and by the Mochida Memorial Foundation for Medical and Pharmaceutical Research. The work is based on results obtained from a project commissioned by the New Energy and Industrial Technology Development Organization (NEDO). K.W. is a member of the Department of Ubiquitous Health Informatics, which is engaged in a cooperative program between the University of Tokyo and NTT DOCOMO. S.Y. is a member of the Department of Prevention of Diabetes and Lifestyle-related Diseases, which is in a cooperative program between the University of Tokyo and Asahi Mutual Life Insurance Company. **Author contributions:** S.O., R.H., Y.K., and M.U. designed the experiments, data analysis, and overall research; S.O. and M.U. developed the setups and performed optical imaging experiments; R.H. developed algorithms for the imaging recovery and data analysis; M.U., S.O., and H.A. modified and used them for the cell analysis with the strong support of I.S.; R.H. and H.N. supervised the work; and S.O., R.H., Y.K., and M.U. wrote the manuscript with the input of the other authors. **Competing interests:** S.O., R.H., and I.S. are the founders and shareholders of ThinkCyte Inc., a company engaged in the development of the ultrafast imaging cell sorter. Y.K., M.U., H.A., K.F., and H.N. have shares of stock options of ThinkCyte Inc. Y.K. and H.A. are employees, M.U. is a former employee, S.O. is a board member, and I.S. is a scientific advisor of ThinkCyte Inc. S.O., R.H., Y.K., I.S., S.Y., K.F., and K.W. are inventors on patent applications submitted by the University of Tokyo and Osaka University covering the motion-based ghost imaging as well as image-free morphology analysis. **Data availability:** Original measurement data and codes for analysis are deposited in Zenodo (*15*), a repository open to the public.

1 October 2018; accepted 3 April 2019
20 Published online 19 April 2019
10.1126/science.aav3136

Downloaded from http://science.sciencemag.org/ on November 19, 2019

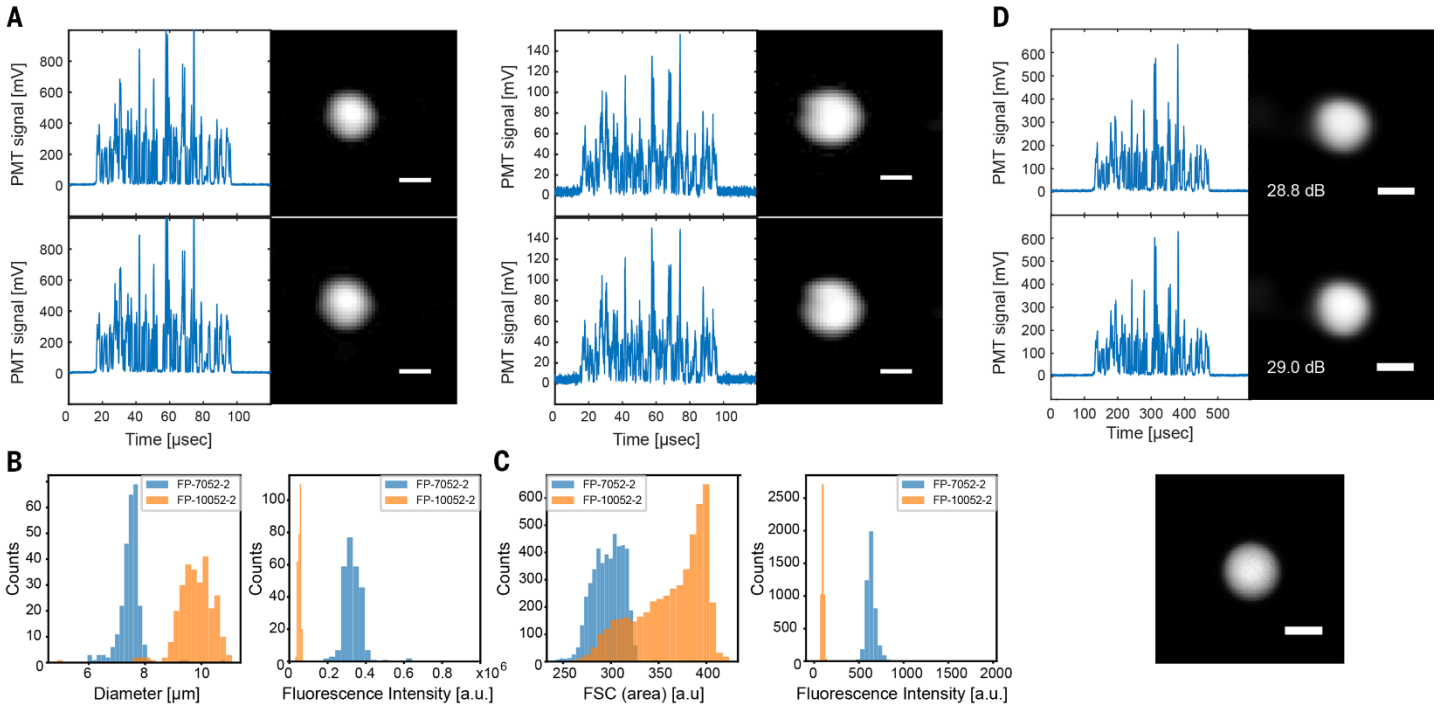

Fig. 1. Fluorescence image reconstruction and analysis in flow implementations of ghost cytometry. (**A**) Pairs of an example compressive waveform generated from fluorescent beads in high-speed flow at a temporal width of <100 μs, and its reconstructed image (cropped after reconstruction). Left and right panels were obtained from different kinds of fluorescent beads [fluorescent yellow particles (FP-7052-2 and FP-10052-2, Spherotech) with mean diameters of 7.4 μm and 10.2 μm, respectively]. (**B**) Left and right panels are histograms of bead diameter and total fluorescence intensity, respectively, obtained from a library of reconstructed single-bead images for the same kinds of beads as in (A), clearly showing the capability of analysis based on the reconstructed images. After cropping the reconstructed images into a size of 32 by 32 pixels, the diameters and total intensities were calculated by applying Canny edge detection and integrating the cropped images, respectively. (**C**) Left and right panels are histograms of forward scattering and fluorescence intensity, respectively, for the same kinds of beads as in (B) obtained by using a commercial flow cytometer (JSAN, Bay Bioscience). The consistency between the histograms in (B) and (C) confirms the imaging capability of GC. (**D**) Top: Example compressive waveforms from fluorescent beads (FP-7052-2) flowing through a PDMS microfluidic device and their reconstructed images (cropped after reconstruction). The flow speed was slowed down in consideration of the stability of the PDMS device. Bottom: A fluorescence image taken by a conventional microscope (Olympus), used as a reference for calculating PSNRs. The image of the reference bead was taken on a slide glass with a 20× objective (UPLSAPO 20×, Olympus) and an arrayed pixel camera (ZWO ASI1600MM). The PSNRs were calculated with images adjusted to scale, cropped to 134 by 134 pixels, and normalized with respect to intensity. All scale bars, 5 μm.

Downloaded from http://science.sciencemag.org/ on November 19, 2019

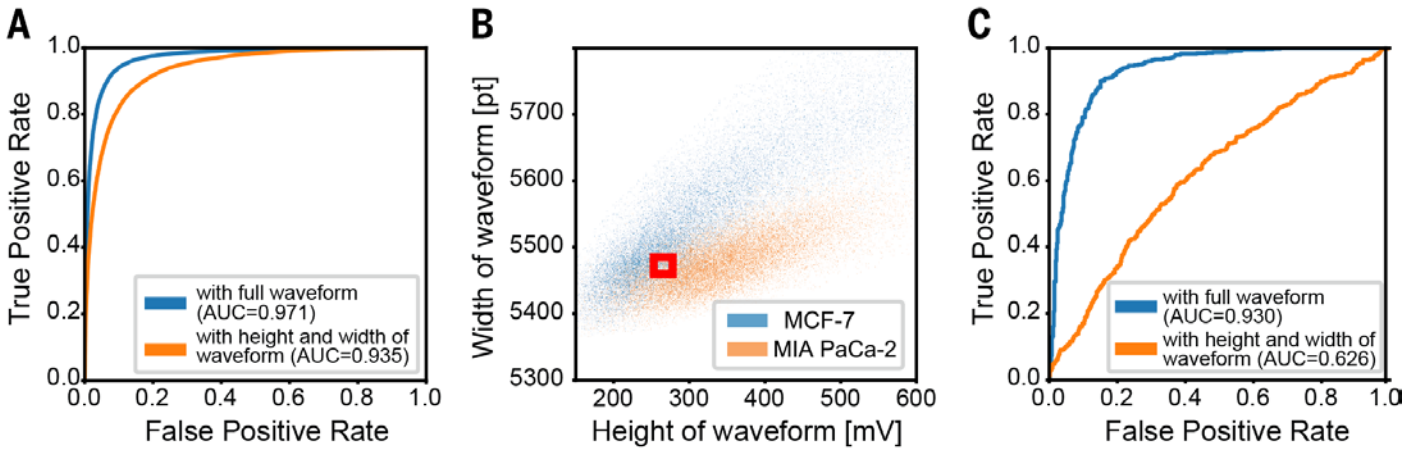

Fig. 2. Comparison of classification results of cells using different features of the waveforms. (**A**) ROC curves when classifying MCF-7 and MIA PaCa-2 cells using GC waveforms directly and two features of peak height and width extracted from the waveforms for the same dataset as in figure 4C of (*1*). With the same training and testing conditions as in (*1*), the AUC for each was 0.971 and 0.935, respectively, showing that the former performs classification of the cells using more information than the two features. (**B**) Scatterplot showing the GC waveform height and width distributions of MCF-7 and MIA PaCa-2 cells for the test data set in (A). The red rectangle shows an area where the populations of the MCF-7 and MIA PaCa-2 cells overlap, of which cells were used for classifications in (C). (**C**) ROC curves using the same training dataset as in (A), but performing classification of only the cells inside the red rectangle in (B); 577 MCF-7 and 524 MIA PaCa-2 cells were used to test the classifier. In the region where the height and width of the GC waveforms are similar, the AUC of the two-feature–based classification dropped to 0.626, whereas the AUC of the whole waveform–based classification robustly remained at a high value of 0.930. These results support the idea that GC performs classification using morphological features included in the waveform more than only the size, fluorescence intensity, or speed of the cells, which appear in the height and width of the waveform.

Downloaded from http://science.sciencemag.org/ on November 19, 2019

Science

Response to Comment on "Ghost cytometry"

Sadao Ota, Ryoichi Horisaki, Yoko Kawamura, Masashi Ugawa, Issei Sato, Hiroaki Adachi, Satoko Yamaguchi, Katsuhito Fujiu, Kayo Waki and Hiroyuki Noji

Science **364** (6437), eaav3136.
DOI: 10.1126/science.aav3136

ARTICLE TOOLS http://science.sciencemag.org/content/364/6437/eaav3136

REFERENCES This article cites 11 articles, 3 of which you can access for free
http://science.sciencemag.org/content/364/6437/eaav3136#BIBL

PERMISSIONS http://www.sciencemag.org/help/reprints-and-permissions

Use of this article is subject to the Terms of Service

Science (print ISSN 0036-8075; online ISSN 1095-9203) is published by the American Association for the Advancement of Science, 1200 New York Avenue NW, Washington, DC 20005. The title *Science* is a registered trademark of AAAS.

Copyright © , American Association for the Advancement of Science

Downloaded from http://science.sciencemag.org/ on November 19, 2019